Available online at www.sciencedirect.com
ScienceDirect
Journal of the European Ceramic Society 30 (2010) 831–838
www.elsevier.com/locate/jeurceramsoc

CeO_2 nano-precipitation in borosilicate glasses: A redox study using EELS

Guang Yang, Stuart Cook, Russell J. Hand, Günter Möbus *

Department of Engineering Materials, University of Sheffield, Sheffield, UK

Received 23 December 2008; received in revised form 11 September 2009; accepted 28 September 2009
Available online 28 October 2009

Abstract

Precipitation of nanoscale phases in a series of five related alkali-borosilicate glasses is studied by scanning transmission electron microscopy and electron energy loss spectroscopy (EELS). All glasses studied are doped with 4 mol% of CeO_2, and contain varying concentrations of other oxides to participate in possible redox interactions, including Fe_2O_3, Nd_2O_3, AgO, and Cr_2O_3. The particular precipitates found vary from droplet shaped amorphous to dendritic shaped single crystals. The oxidation state of Ce and the existence and morphology of Ce precipitates is found to depend on both cooling sequence and the presence of other oxides. One aim of the study is to explore and showcase the applicability of high spatial resolution fine structure EELS for the study of the interrelated phenomena of redox interaction, phase separation, solubility, and nanoscale crystallization.

Keywords: Nanocomposites; Glass; Electron microscopy; Crystallization

1. Introduction

Alkali-borosilicate glasses have been studied for several decades. A significant part of past research is motivated by the vitrification of nuclear waste at industrial scale.[1] Under standard conditions, waste elements are immobilised by chemical bonding into the glass structure, however if the chemical solubility is exceeded, precipitation of a range of crystal sizes and shapes, ranging from volume distributed nanoparticles to macroscopic surface crystals will occur. This could negatively influence immobilization performance if the precipitation reduces the durability of the residual glass matrix composition, or if melter performance becomes affected by gravity induced separation of heavier particles.[2,3] On the other hand, if the precipitates and residual glass phase are both resistant to leaching by water and/or there is a homogeneous volume distribution of particles below the percolation threshold, safe immobilization can be expected even in the presence of such particles. Because of the higher waste-loading factor achievable, such deliberate multi-phase glass/particle composites have recently attracted renewed attention as glass-composite materials (GCM) for nuclear waste immobilization.[2–6] The study of precipitation mechanisms in alkali-borosilicate glasses is therefore equally important for unwanted and for deliberately nucleated phases. In the current study, we concentrate on the immobilization of Ce, which is commonly used as an actinide surrogate. Apart from Hf, Ce is the most commonly used surrogate for Pu, referring to ion radius and multi-valence, see e.g. 2,7 for details. We study the precipitation and oxidation states of Ce as a function of other possible reduction–oxidation (redox) partner dopant elements and also the mutual influence of Ce and Ag precipitation. This study is meant as a first step towards a simultaneous evaluation of valence of all multi-valent elements. All surrogate elements are selected to be typical representatives of a multi-element waste stream, e.g. Ag is often chosen to represent the Pt-group and noble-metal elements in a simplified waste glass.

In the non-nuclear field applications of Ce-doping and precipitation are equally important. The multiple valence (+3/+4) and precipitation mechanism of Ce has a broad range of relevance for glass or glass/ceramic research, as Ce-doped glasses are used in the optical field, e.g. for UV absorption, opacification, or photochromic applications, and also as a nucleation agent to generate noble-metal particle nanocomposites, or to enhance nucleation and crystallization in glass ceramics.[8–10]

Multiple multi-valent elements will have mutual redox interactions in the glass melt, which can influence the solubility and oxidation states of elements in the final products.[11–13] During glass melting, the equilibrium between redox states of the multiple component oxides is complex and depends on the base glass composition as well as the melting environment and

* Corresponding author. Tel.: +44 114 2225512.
E-mail address: g.moebus@sheffield.ac.uk (G. Möbus).

0955-2219/$ – see front matter © 2009 Elsevier Ltd. All rights reserved.
doi:10.1016/j.jeurceramsoc.2009.09.024

conditions.[14–16] In general, the redox equilibrium for a single multi-valent element can be expressed as[17]:

$$4M^{n+} + 2mO^{2-} \Leftrightarrow 4M^{n-m} + mO_2(\text{gas}), \quad (1)$$

where M denotes the redox-active element, n is the charge of the oxidised species and m is the number of electrons transferred to the reduced state. For an element added in a more oxidised state, the element can be reduced to lower oxidation states (e.g. Ce^{4+} to Ce^{3+}) and O_2 will be generated (reaction (1) goes from left to right). For elements added in the reduced state, the oxygen can oxidise the element to a higher oxidation state (equation goes from the right to the left). Reaction (1) also depends on several parameters including the melt temperature, time, oxygen partial pressure, melt composition and the concentration of the elements in the melt.[12]

Various spectroscopy techniques, including optical, X-ray photoelectron spectroscopy (XPS), electron spin resonance (ESR), nuclear magnetic resonance (NMR), Raman or X-ray absorption spectroscopy/extended X-ray absorption fine structure (XAS/EXAFS) are suitable for the assessment of the accommodation of dopant atoms in glasses. Our choice to use transmission electron microscopy (TEM) based energy loss spectroscopy (EELS) and in particular energy loss near edge structure (ELNES) for this purpose is motivated by the possibility of using these spectroscopy techniques with a simultaneous acquisition of nanoscale images. The formation of sub-100 nm sized precipitates can then be observed within the same electron microscope session using high-resolution (HREM) or annular dark field scanning modes (ADF-STEM) as imaging techniques. Due to the high spatial resolution of EELS-based analytical TEM, with beam size down to 1 nm, the Ce valence can be determined locally by continuous line-scans crossing regions of the glass matrix and selected precipitates. In the particular case of lanthanides, valence measurements by EELS have been pioneered first for ceramic minerals,[18] and more recently for glasses,[19,20] and also to study irradiation induced valence change on the surfaces of free-standing particles of ceria.

Our aim is to determine the Ce valence in glass and precipitates for a series of five simulated nuclear waste glasses all doped with 4 mol% CeO_2, and with varying concentrations of other dopant elements.

2. Experimental work

2.1. Glass specimen preparation

Five glass samples of doped alkali-borosilicate glass (ABS) were produced (see Table 1). Reagent grade SiO_2, H_3BO_3, Li_2CO_3, Na_2CO_3, K_2CO_3, CeO_2, Cr_2O_3 and ZrO_2 were batched to give a 300 g glass melt and mixed before transferring into a Pt crucible. All starting materials were melted at 1400 °C in an electric furnace for 5 h with 1 h unstirred melting and 4 h stirring. After melting, all the glass melts were poured into a preheated steel mould to form a rectangular glass block approximately 2 cm × 2 cm × 10 cm in size. This block was then transferred to a furnace for annealing at 570 °C for 1 h and then cooled to room temperature at the rate of 1 °C/min to relieve the stresses in the glasses. Specimens for TEM were prepared by crushing a randomly selected interior fraction of the bulk sample in an agate mortar and pestle with acetone. Some suspended particles were transferred onto a carbon-film on a TEM copper grid.

Table 1
Batched glass composition (mol%).

	NLBS-CCZ	KBS-CCZ	KBS-CFC	KBS-CH	KBS-ACFN
SiO_2	51.4	51.4	51.4	51.4	60
B_2O_3	25.7	25.7	25.7	25.7	15
Na_2O	8.6	–	–	–	–
Li_2O	4.3	–	–	–	–
K_2O	–	12.9	12.9	12.9	15
Ag_2O	–	–	–	–	1
ZrO_2	4	4	–	–	–
CeO_2	4	4	4	4	4
Cr_2O_3	2	2	2	–	–
Fe_2O_3	–	–	4	–	3
HfO_2	–	–	–	6	–
Nd_2O_3	–	–	–	–	2

2.2. HREM/STEM and EELS/ELNES

A JEOL 2010F Field Emission Gun TEM with an accelerating voltage of 200 kV was used for all of the analysis, except for Fig. 4. With a 200 kV accelerating voltage, an image resolution of ~1.9 Å is theoretically achievable. The energy spread of the electron beam is about 1 eV or less, which gives the opportunity to achieve good electron energy loss spectra. Some high-resolution electron microscopy (HREM) analysis was performed to establish crystalline versus amorphous nature of nano-precipitates. Mostly, scanning TEM mode with annular dark field detector (ADF-STEM) was preferred as this mode collects the transmitted electrons which undergo scattering through large angles giving high contrast with bright precipitates (that contain high-Z atoms, e.g. Ce or Ag) on a dark glass matrix (average low-Z).

Electron energy loss spectroscopy (EELS) signals were obtained using a Gatan Image Filter (GIF). The full width at half maximum (FWHM) of the zero loss peak at the energy dispersion of 0.2 eV/pixel was 1.6–1.8 eV. In order to minimise the electron irradiation damage on the glasses and at the same time achieve good enough signal-to-noise ratio (SNR) for quantification, each spectrum was integrated from 4 or 5 individual spectra with 2 s exposure time each. The spectrum acquisition time is similar to those used in previously reported irradiation tests on borosilicate glass,[19] however, no irradiation damage was observed within the Ce-M-edge region after the spectrum acquisition for all the simulated nuclear waste glasses studied here. The background was subtracted from the spectra using Digital Micrograph software with a power law model.

In order to identify the valence states of Ce in different phases, electron energy loss near edge structure (ELNES) was used. For lanthanides, the intensity ratio of the M-edge transition lines M_5/M_4 ("white lines") has linear relationship with valence,[21,22] thus by comparing the white line ratios with Ce reference spectra

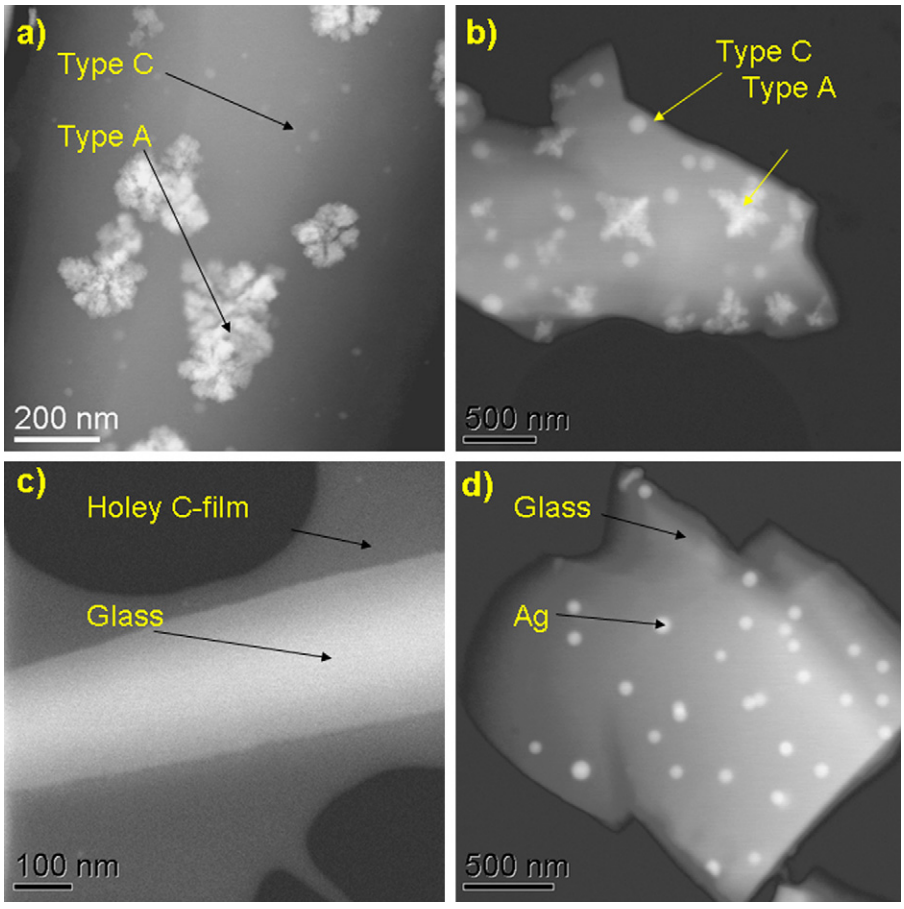

Fig. 1. ADF-STEM images of 4 glasses with acronyms and numbers as detailed in Table 1 and "Type index" of particles superimposed as detailed in Section 3.1. (a) NLBS-CZC, (b) KBS-CZC, (c) KBS-CH and (d) KBS-ACFN.

for compounds with known single Ce valence, the unknown Ce valences of different phases can be obtained. The data processing method selected for quantifying the line ratio is the "second derivative method",[21] which integrates peak areas between zero crossings after double-differentiating the original spectrum. The second derivative method was reported to be less sensitive to the energy resolution as well as the thickness of the sample, which are points of concern in our experiments because all glass fragments are non-flat and multiple scattering may introduce artifacts.

3. Results and discussion

3.1. Morphology of precipitates

Crystallization was found in all glasses except the Cr and Fe-free KBS-CH glass. This was determined by a combination of X-ray powder diffraction and by electron diffraction on individual separated phases as seen in TEM images. Since Ce solubility in simulated nuclear waste glasses is known to be melting temperature dependent,[23] all glasses have been melted at the same temperature.

In all Cr-containing glasses, due to the low solubility of Cr in ABS glasses, large amounts of Cr separated into micron-sized Cr_2O_3 crystals. Ce was found either to precipitate into differently shaped crystals or was found to fully dissolve; this depends on the glass composition as well as other added oxides. The glass matrix was initially homogeneous by HREM and X-ray diffraction patterns, although prolonged deliberate high-dose electron irradiation could trigger nanoscale phase separation.[24]

Ce was found in the glass matrix of all of the five samples while Ce-rich crystals were found in three of the glasses, NLBS-CCZ, KBS-CCZ and KBS-CFC. Metallic Ag was the only precipitate found in the KBS-ACFN glass, while all Fe_2O_3, HfO_2 and Nd_2O_3 was dissolved in the respective glasses. Fig. 1 shows the annular dark field images of fragments from the four different glasses other than the KBS-CFC glass. Ce-containing particles and metallic Ag are visible with high Z-contrast.

In NLBS-CCZ and KBS-CCZ glasses (Fig. 1a and b), the choice of alkali species was the only change in glass composition, and it was found that there is no distinct morphological difference between the Ce precipitates in both glasses. In the KBS-CH and KBS-ACFN glasses, no Ce precipitates were found (the bright dots in Fig. 1d were found to be metallic Ag) and it can be concluded that CeO_2 was fully dissolved in the glass matrix. In KBS-CFC glass, however, the Ce precipitation was more complex and differences were seen not only in morphology but also in crystallinity, thus this glass is shown separately in Fig. 2. There are three kinds of precipitates in the KBS-CFC glass, all of which are Ce-rich phases as confirmed by EDS and

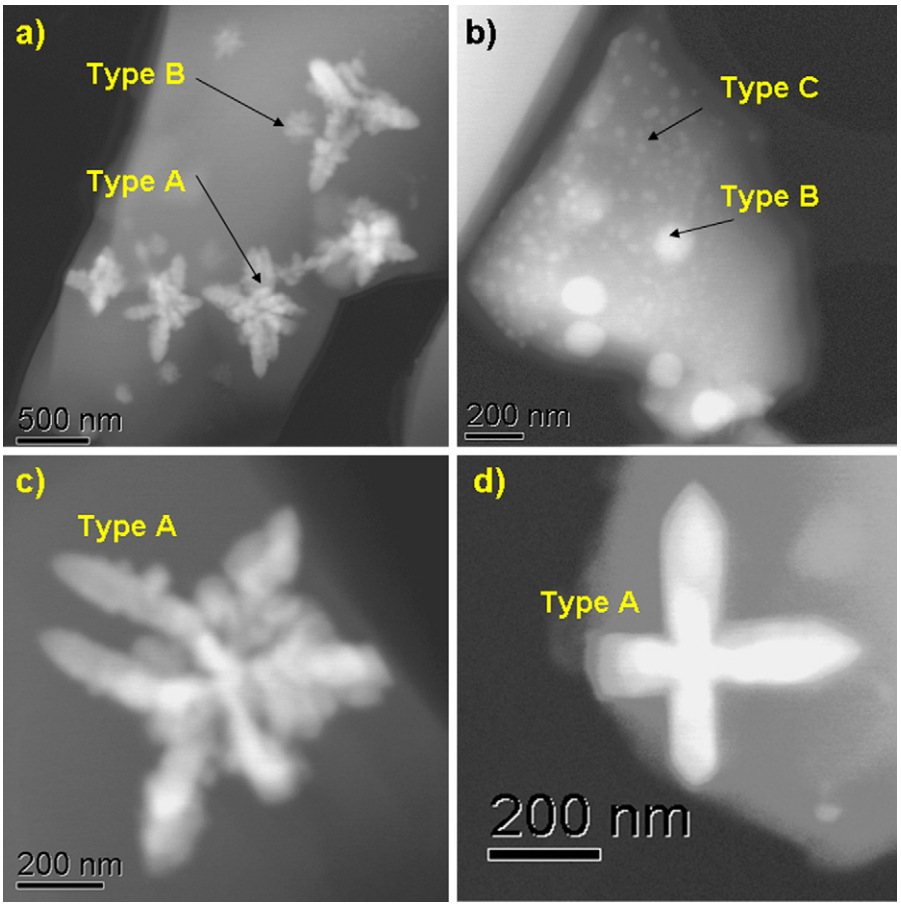

Fig. 2. ADF-STEM images of 4 groups of precipitates from KBS-CFC glass: (a) Type A, and Type B particles, (b) Type B and Type C particles, (c and d) Type A dendrites of different branching/fractal morphology.

EELS. We discriminate three types of phases by their mean size and their structure (crystal versus amorphous):

Type A: 200–500 nm precipitates of pronounced dendritic structures (Fig. 2a, c and d). They were confirmed as single crystals by electron diffraction (as expected) and had a cubic (fluorite) crystal structure. Similar particles were found in the related glasses, however their equivalent diameter varies with glass type being 200–400 nm in NLBS-CCZ glass and 200–600 nm in KBS-CCZ glass. The branching statistics are quite diverse (Fig. 2c and d), which may correspond to a different growth stage of precipitates.[25] Some particles show primary branches only, while most have a more extensive fractal appearance. The growth orientation of all primary branches was ⟨1 0 0⟩. A detailed crystallographic and morphological analysis of such a typical nanodendrite is presented in Ref. 35.

Type B: 100–150 nm roundish particles/phases, which appeared amorphous in HREM and electron diffraction. They were Ce-rich and found exclusively in the KBS-CFC glass and not in any other of the studied compositions (Fig. 2b, large particles).

Type C: 10–50 nm roundish particles/phases, which were again amorphous. These were common features found in the NBS-CCZ, KBS-CCZ and KBS-CFC glasses and were also Ce-rich (Fig. 2b, small particles).

All observed particles were distributed randomly and homogeneously throughout the glass blocks, with the exception of some CeO_2 dendrites that had grown on Cr_2O_3-plates (present in some glasses), see Section 3.3.1 below.

3.2. Spectroscopy

The Ce-M-edge fine structure was selected from the EELS spectrum and recorded for all glasses and for selected particles within the glasses. For dendrites the Ce signal was very strong and the scatter in the M_5/M_4 ratios was small. However, for spectra acquired from the glass matrix as well as from the amorphous particles, due to the comparatively low content of Ce, the signal-to-noise ratio was low. In this case, several spectra were averaged to improve the signal-to-noise ratio and to provide a satisfactory result. Fig. 3 shows the second derivative data of selected spectra. As published before,[26,27] the reference M_5/M_4 ratios, measured under identical instrumental conditions, were 0.9 for Ce^{4+} and 1.3 for Ce^{3+}, respectively. By interpolating the measured M_5/M_4 ratios from the boundary values defined by the reference materials, the calculated formal Ce valences were obtained; see Table 2. A fractional formal valence is to be understood as a distribution of both Ce^{3+} and Ce^{4+} along the electron beam path through the specimen, which could realistically exist at specific temperatures and redox partner concentrations. How-

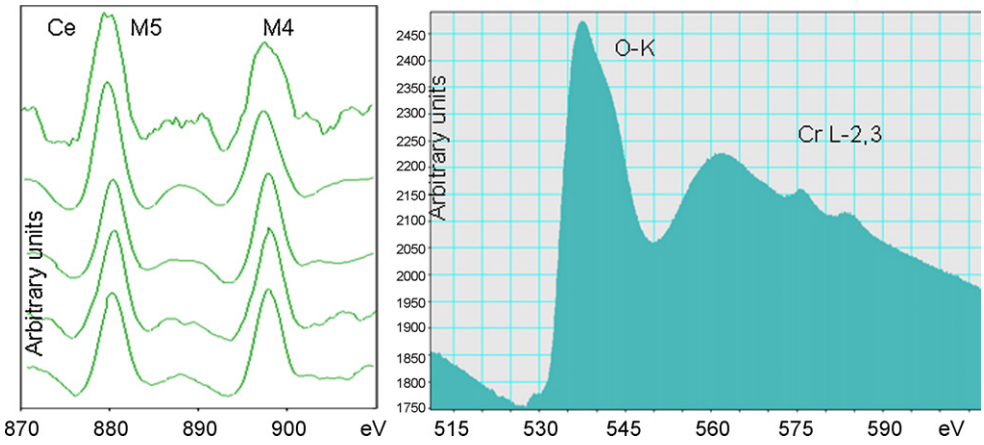

Fig. 3. (a) Second derivative EELS spectra of Ce $M_{5,4}$ white lines for (i–v): top to bottom—(i) glass matrix of KBS-CFC glass, (ii) ~100 nm spherical particles in KBS-CFC glass, (iii) dendrites in KBS-CFC glass, (iv) glass matrix of KBS-CH glass, (v) glass matrix of KBS-ACFN glass; horizontal axis: energy loss from 870 to 910 eV; vertical axis: 2nd derivative of intensity (a.u.). To avoid calibration errors, all spectra are energy fitted to have the first peak (M5) coincident. (b) O-K-edge and Cr-L-edge superimposed.

ever, for particles clearly smaller than the specimen thickness, fractional data more likely indicate overlap of particle and glass matrix and require correction. Accuracy of ELNES quantification is often limited by the energy calibration, e.g. for inner shell edges of transition metal elements (L-edges). However, the quantification of Ce-edges in comparison is fairly robust as it relies mainly on a ratio of intensities of peaks. There is also a small chemical shift of Ce-M-edge with valence (see e.g. 27), however, this effect is not evaluated in this work, and all 5 spectra are matched in their M5 energy position. The only parameter extracted is the peak area ratio.

The desirable parallel evaluation of Cr valence via ELNES L2,3 peak ratios is omitted, as motivated by Fig. 3b. The problem is that the Cr-L-edge sits marginally on the dominating O-K-edge due to only <2% of Cr-oxide content. Without ability of precise background subtraction and precise evaluation of chemical shifts, any Cr valence evaluation would be unreliable.

3.3. Interpretation and discussion

Ce valences varied between different glasses and precipitates. All dendritic precipitates, irrespective of morphology, were pure CeO_2 crystals. The Ce-rich spherical amorphous particles, however, displayed different valences. They occurred in a bi-modal size distribution (which can be directly deduced by visual inspection of the micrographs). The Ce valence state also differed in the glass matrices.

Table 2
Ce valences evaluation in different glasses using second derivative method.

Glass	Ce phase	Formal valence	Corrected valence
NLBS-CCZ	Dendritic crystal	4.0	4.0
	Glass matrix	3.1	3.1
KBS-CCZ	Dendritic crystal	3.9	4
	Glass matrix	3.1	3.1
KBS-CFC	Dendritic crystal	4.0	4.0
	Big spherical particle	3.0	3.0
	Small spherical particle	3.4	~4.0
	Glass matrix	3.0	3.0
KBS-CH	Glass matrix	3.9	~4.0
KBS-ACFN	Glass matrix	3.9	~4.0

3.3.1. NLBS-CCZ and KBS-CCZ glass

In both glasses, three metal oxides were added to this batch: CeO_2, Cr_2O_3 and ZrO_2. Zr has only one valence state and therefore does not participate in the redox interactions. Two multi-valent elements were present with Ce having +3 and +4 valences and Cr +6, +3 and +2. The redox pair involved with Cr is not obvious. Oxidation to Cr^{6+} in such glasses is quoted to depend on the presence of strong oxidants in the glass melt.[28] On the other hand, Cr3+/Cr6+ has a very close standard potential to Ce4+/Ce3+, while Cr3+/Cr2+ is at the opposite extreme.[11,12] Cr2+ would therefore practically not coexist with Ce4+ in order to enter a mutual redox change between Cr and Ce, although melting happened in air.

At this point it is essential to discuss phase separation: phase separation related phenomena in this glass can be seen on two length scales—the existence of round "droplet" shaped Ce-rich phases of around 20 nm diameter could be seen as a first phase separation, which by EDX and EELS could only be confirmed as highly Ce-oxide rich. Due to its diameter being smaller than the specimen thickness, geometric overlap with the matrix is unavoidable in these measurements. We assume from the visual impression, that the matrix phase left behind after this first phase separation is non-separated alkali-borosilicate. As reported elsewhere, intense electron beam irradiation for 3 min is known[30] to artificially induce phase separation. This could be confirmed for this glass even as its composition is outside the "vycor" phase separation region in the ternary A–B–S diagram.[36]

In order to clarify the timing of crystal formation and phase separation some further accompanying experiments have been carried out as follows: a glass melt was split into three cooling sequences—(i) quenching a part of the melt in water, (ii) annealing with our standard procedure (1 h, 570°, as used for all our glasses), and (iv) annealing at 2 h, 600°, see Fig. 4.

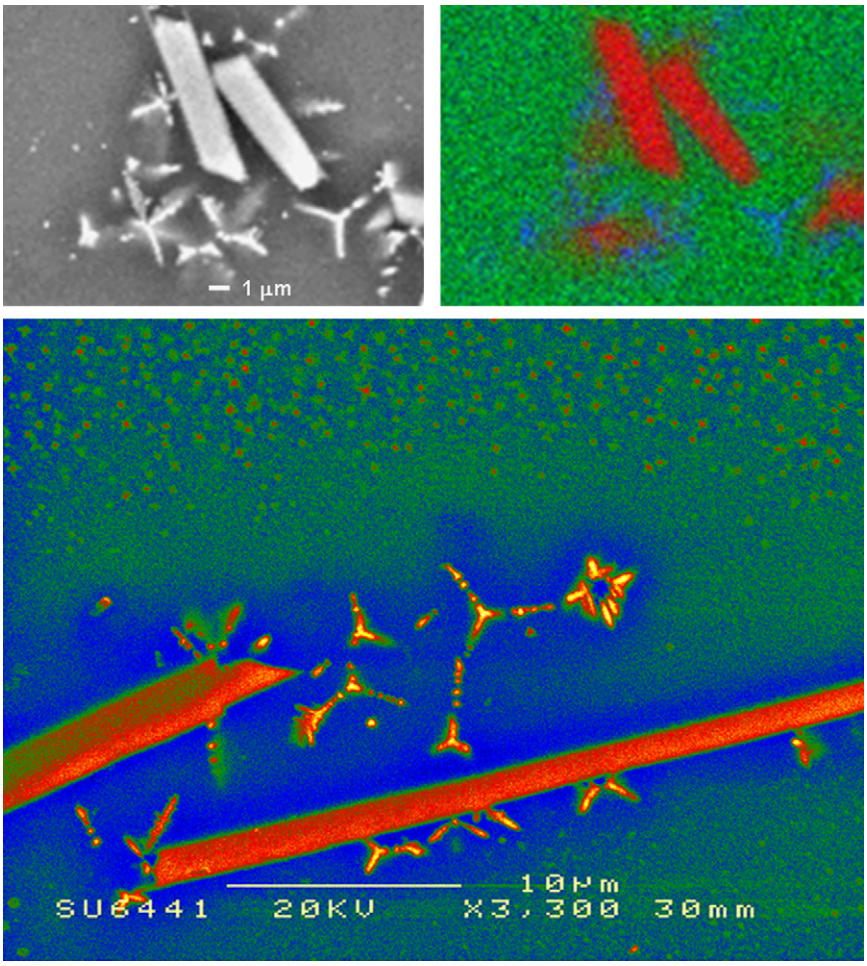

Fig. 4. Annealing and cooling of glass NLBS-CCZ: comparison of two sequences—(a) 570°, 1 h annealing, and (b) 600°, 2 h annealing with precipitate growth doubled in size. (For interpretation of the references to color in this figure legend, the reader is referred to the web version of the article.)

It is found that the quenched glasses are lacking the crystalline precipitates, as well as the phase separated Ce-oxide rich droplet phase. Amongst the two annealing sequences, growth of the dendritic particle diameter by longer annealing is the main difference, while the occurrence of crystals and amorphous droplets as such is in common.

3.3.2. KBS-CFC glass

Three redox-active elements were included in the KBS-CFC glass: Ce, Fe and Cr. All of them have at least two valence states. The addition of Fe_2O_3 introduces further competing redox reactions, e.g. between Ce and Fe and/or between Fe and Cr.

Fe^{2+} has been reported to unlikely coexist with Ce^{4+} in the glass melt at low concentrations[28] due to the mutual redox interactions, however above 2 mol%, as in our case, the relationships are more complicated,[11,29,31–34] and multiple Fe-valences could coexist. This becomes even more complex if the molar ratios of cations are not equal. Originally the same amounts of CeO_2 and Fe_2O_3 were added to the batch but CeO_2 precipitated as crystals, thus it was estimated that at least twice more Fe remained in the glass matrix than Ce. EELS analysis has shown that the Ce valence was nearly +3, while Fe-L-edge-EELS was at least consistent with +3 valence, although the low concentrations did not allow safe Fe-ELNES quantification. The greater diversity of possible redox interactions might explain the more complex precipitation morphology seen in this glass, while the main crystalline phase was still CeO_2, as confirmed by EELS.

We base the suspected influence of Cr on the Ce precipitation and oxidation state in both the glasses NLBS-CCZ and KBS-CFC mainly on the observation of precipitation images in scanning electron microscopy (SEM): due to the low solubility of Cr, large amounts of Cr precipitated as Cr_2O_3 needles of many microns in size in this glass, see Fig. 5. It can be seen that the large Cr-oxide crystals are surrounded by some dendritic CeO_2 as a surface-precipitation phenomenon catalyzed by Cr-oxide. After a ~5 µm wide Ce depletion zone around the Cr-oxide needles, the typical random distribution of Ce-oxide nanoparticles is seen (upper end of Fig. 5c), which are also visible in TEM. All the remaining Cr was totally dissolved in the glass matrix without nano-precipitation. Identification of chemistry in the SEM samples was obtained via EDX chemical mapping (Fig. 5b).

3.3.3. KBS-CH glass and KBS-ACFN glass

These two glasses are discussed together because in both cases the Ce in the glass was found to be in the +4 valence state, and no Ce-containing precipitates formed in these glasses.

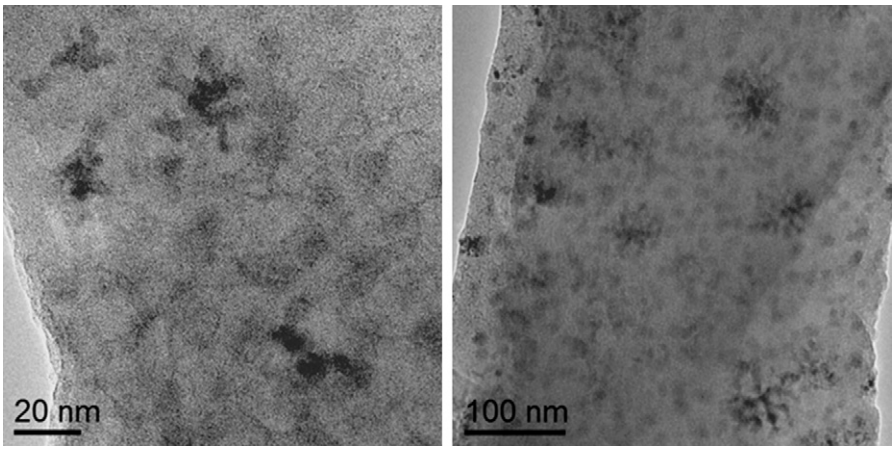

Fig. 5. SEM micrograph of Cr_2O_3 needle shaped micro-precipitates in the KBS-CFC glass by secondary electron imaging (a) and 3 channel EDX mapping (b) with red = Cr, green = K, blue = Ce. The secondary crystals of dendritic shape on the needle surface or in the vicinity are CeO_2. (c) An extended backscattered electron view, enhancing the Ce-free depletion zone, outside of which CeO_2 nanocrystals (Type A of Fig. 1a) are finely dispersed (pseudo-color for contrast enhancement, not a chemical map).

KBS-CH contained only one multi-valent element, thus no redox mutual reaction other than reaction (1) took place during melting. In this case the addition of Hf may have influenced the solubility of Ce^{4+}, making Ce^{4+} the preferred state in this glass allowing total dissolution. The other possibility is that the base glass composition favours high solubility of Ce^{4+} as long as there is no other redox-active element present to drive the redox equilibrium towards Ce^{3+}. Unlike for the NLBS-CCZ, KBS-CCZ and KBS-CFC glasses there is no other metal cation to be oxidised by Ce.

Ag is relatively easy to reduce[11] and has been found as metallic precipitates in previous simulated nuclear glasses.[34] Therefore the generation of metallic Ag particles in the glass was expected. Literature about Ce/Ag systems in glasses,[8] mostly for optical applications, e.g. Ag–Ce-doped laser glasses, does not fully resolve how essential the role of Ce is in driving Ag into reduced metallic state. A redox connection between Ce and Ag is very well possible in our case. The addition of single valence Nd_2O_3 is another possible factor that influences the Ce^{4+} solubility in glasses.

3.3.4. Further work

In the present work, only Ce is directly evaluated for valence. A measurement of valence of other elements apart from Ce is desirable as future work, however, this will require either to swap Cr for another redox partner (e.g. Mn) to avoid overlap with O-K-edges, or to even further reduce the number of glass components, such that one pair can be studied at a time.

4. Conclusions

Five Ce-loaded simplified nuclear waste glasses were studied and Ce valence states were estimated. The aim of this work is to combine four fields of glass chemistry and microstructure analysis: (i) solubility studies, (ii) redox studies, (iii) nucleation and crystallization and (iv) nanoscale phase separation studies, into one methodology using one instrument. STEM imaging and EELS fine structure analysis are the signals. It was found that Ce was accommodated in both its valences within the up to four different phases identified, including crystalline dendrites and amorphous droplets of different size regime and also including the residual depleted glass matrix. The dendrites have a Ce (IV) fluorite structure as confirmed by electron diffraction.[35] However, in two glasses, all Ce dissolved in the glass and then the valence remained at +4, as in the batched CeO_2. In total, the findings provide some evidence, that the Ce valence, which has been quoted before[13,21,23] to respond to the temperature and oxidation/reduction environment in the melt, glass matrix composition, and total Ce loading, has also a distinct dependence on the presence of other multi-valent elements at concentrations of several mol%, and on precipitation of crystals (whether direct or indirect via change of the residual glass composition).

The exploration of the three interlinked phenomena of (i) nanoscale crystallization, (ii) glass-in-glass phase separation and (iii) redox interaction is complicated, and a main point of our work is to explore, whether STEM + EELS could provide a unique solution to this family of problems due to its high spatial resolution, while being valence sensitive at the same time.

References

1. Lutze, W. and Ewing, R. C., *Radioactive Wasteforms for the Future*. North Holland, Amsterdam, 1988.
2. Ojovan, M. I. and Lee, W. E., *An Introduction to Nuclear Waste Immobilisation*. Elsevier, Amsterdam, 1995.
3. Li, H., Hrma, P., Vienna, J. D., Qian, M., Su, Y. and Smith, D. E., Effects of Al_2O_3, B_2O_3, Na_2O, and SiO_2 on nepheline formation in borosilicate glasses: chemical and physical correlations. *J. Non-Cryst. Solids*, 2003, **331**, 202–216.
4. Lee, W. E., Ojovan, M. I., Stennett, M. C. and Hyatt, N. C., Immobilisation of radioactive waste in glasses, glass composite materials and ceramics. *Adv. Appl. Ceram.*, 2006, **105**, 3–12.
5. Digeos, A. A., Valdez, J. A., Sickafus, K. E., Atiq, S., Grimes, R. W. and Boccaccini, A. R., Glass matrix/pyrochlore phases for nuclear wastes encapsulation. *J. Nucl. Mater.*, 2004, **327**, 148–158.
6. Loiseau, P., Caurant, D., Baffier, N., Mazerolles, L. and Fillet, C., Glass-ceramic nuclear waste forms obtained from SiO_2–Al_2O_3–CaO–ZrO_2–TiO_2 glasses containing lanthanides (Ce, Nd, Eu, Gd, Yb) and actinides (Th): study of internal crystallization. *J. Nucl. Mater.*, 2004, **335**, 14–32.

7. Bingham, P. A., Hand, R. J., Stennett, M. C., Hyatt, N. C. and Harrison, M. T., The use of surrogates in waste immobilization studies: a case study of plutonium. In *Mater. Res. Soc. Symp. Proc., Sci. Basis for Nuclear Waste Management XXX*, 2008, p. 1107.
8. Dai, Y., Qui, J., Hu, X., Yang, L., Jiang, X., Zhu, C. and Yu, B., Effect of cerium oxide on the precipitation of silver nanoparticles in femtosecond laser irradiated silicate glass. *Appl. Phys. B*, 2006, **84**, 501–505.
9. Shi, Z. M., Liang, K. M., Zhang, Q. and Gu, S. R., Effect of cerium addition on phase transformation and microstructure of cordierite ceramics prepared by sol–gel method. *J. Mater. Sci.*, 2007, **36**, 5227–5230.
10. Hu, A. M., Liang, K. M., Zhou, F., Wang, G. L. and Peng, F., Phase transformations of Li_2O–Al_2O_3–SiO_2 glasses with CeO_2 addition. *Ceram. Int.*, 2005, **31**, 11–14.
11. Rüssel, C., Redox behavior and electrochemical behavior of glass melts. In *Properties of Glass Forming Melts*, ed. L. D. Pye, A. Montenero and I. Joseph. Taylor&Francis, LLC, Boca Raton, FL, USA, 2005.
12. Schreiber, H. D. and Balazs, G. B., An electromotive force series for redox couples in a borosilicate melt: the basis for electron exchange interactions of the redox couples. *J. Non-Cryst. Solids*, 1985, **71**, 59–67.
13. Paul, A. and Douglas, R. W., Cerous-ceric equilibrium in binary alkali borate and alkali silicate glasses. *Phys. Chem. Glasses*, 1965, **6**, 207–211.
14. Kumar, A. and Singh, S. P., Oxygen-ion activity and its influence on redox equilibria in a ternary soda–lime–silica glass system. *Glastech. Ber.*, 1992, **65**, 69–72.
15. Schreiber, H. D., Merkel, R. C., Schreiber, J. V. L. and Balazs, G. B., Mutual interactions of redox couples via electron exchange in silicate melts: models for geochemical melt systems. *J. Geophys. Res.*, 1987, **92**(B9), 9233–9245.
16. Paul, A. and Douglas, R. W., Mutual interaction of different redox pairs in glass. *Phys. Chem. Glasses*, 1966, **7**, 1–13.
17. Johnston, W. D., Oxidation–reduction equilibria in molten Na_2O–$2SiO_2$ glass. *J. Am. Ceram. Soc.*, 1965, **48**, 184–190.
18. Garvie, L. A. J. and Buseck, P. R., Determination of Ce4+/Ce3+ in electron-beam-damaged CeO_2 by electron energy-loss spectroscopy. *J. Phys. Chem. Solids*, 1999, **60**, 1943–1947.
19. Jiang, N., Qiu, J. and Spence, J. C. H., Long-range structural fluctuations in a CaO–Al_2O_3–$2SiO_2$ glass observed by spatially resolved near-edge spectroscopy. *Phys. Rev. B*, 2002, **66**, 054203.
20. Yang, G., Möbus, G. and Hand, R. J., EELS study of boron coordination in alkali borosilicate glasses under extensive electron irradiation. *Phys. Chem. Glasses: Europ. J. Glass Sci. Technol. B*, 2006, **47**, 507–512.
21. Fortner, J. A., Buck, E. C., Ellison, A. J. G. and Bates, J. K., EELS analysis of redox in glasses for plutonium immobilization. *Ultramicroscopy*, 1997, **67**, 77–81.
22. Egerton, R. F., *Electron Energy-Loss Spectroscopy in the Electron Microscope* (*2nd ed.*). Plenum Press, New York, 1996.
23. Lopez, C., Deschanels, X. and Bart, J. M., Solubility of actinide surrogates in nuclear glasses. *J. Nucl. Mater.*, 2003, **312**, 76–80.
24. Sun, K., Wang, L. M. and Ewing, R. C., Analytical electron microscopy study of electron radiation damage in iron phosphate glass waste forms. *Mater. Res. Soc. Symp. Proc.*, 2003, **757**, II5.3.
25. Haxhimali, T., Karma, A. and Gonzales, F., Orientation selection in dendritic evolution. *Nat. Mater.*, 2006, **5**, 660–664.
26. Yang, G., Möbus, G. and Hand, R. J., Fine structure analysis of glasses and glass composites. *J. Phys.: Conf. Ser.*, 2006, **26**, 73–76.
27. Yang, G., Möbus, G. and Hand, R. J., Cerium and boron chemistry in doped borosilicate glasses examined by EELS. *Micron*, 2006, **37**, 433–441.
28. Doremus, R. H., *Glass Science* (*2nd ed.*). John Wiley & Sons Inc., New York, 1994.
29. Donald, S. B., Swink, A. M. and Schreiber, H. D., High-iron ferric glass. *J. Non-Cryst. Solids*, 2006, **352**, 539–545.
30. Sun, K. *et al.*, Electron irradiation induced phase separation in a sodium borosilicate glass. *Nucl. Instrum. Methods Phys. Res. Sect. B: Beam Interact. Mater. Atoms*, 2004, **218**, 368–374.
31. Yang, G., *Ph.D. Thesis*, University of Sheffield, UK, 2007.
32. Schreiber, H. D., Lauer, H. V. and Thanyasiri, T., Oxidation–reduction equilibria of iron and cerium in silicate glasses: individual redox potentials and mutual interactions. *J. Non-Cryst. Solids*, 1980, **38 and 39**, 785–790.
33. Zamoryanskaya, M. V. and Burakov, B. E., Feasibility limits in using cerium as a surrogate for plutonium incorporation in zircon, zirconia and pyrochlore. *Mater. Res. Soc. Symp. Proc.*, 2001, **633**.
34. Short, R. J., Hand, R. J., Hyatt, N. C. and Möbus, G., Environment and oxidation state of molybdenum in simulated high level nuclear waste glass compositions. *J. Nucl. Mater.*, 2005, **340**, 179–186.
35. Xu, X., Saghi, Z., Yang, G., Hand, R. J. and Möbus, G., Three-dimensional structure of CeO_2 nanodendrites in glass. *Cryst. Growth Des.*, 2008, **8**, 1102–1105.
36. Möbus, G., Yang, G., Saghi, Z., Xu, X., Hand, R. J., Pankov, A. and Ojovan, M. I., Electron irradiation and electron tomography studies of glasses and glass nanocomposites. *Mater. Res. Soc. Symp. Proc.*, 2008, **1107**, 239–245.